Skin Friction Drag Reduction over Staggered Three Dimensional Cavities

Erwin R. Gowree[1], Chetan Jagadeesh[2] and Christopher J. Atkin[2]
[(1)]*Dept. of Aerodynamics, Energetics and Propulsion, ISAE-SUPAERO, Université de Toulouse, France*
erwin-ricky.gowree@isae-supaero.fr
[(2)]*Dept. of Mechanical Engineering and Aeronautics, City, Universiy of London, UK*
chris.atkin.1@city.ac.uk

ABSTRACT

The effect of three-dimensional staggered circular cavities on a zero-pressure gradient incompressible turbulent boundary layer was studied. Two key parameters were varied, being the ratio of the diameter, d, to the depth, h, of the cavity, d/h and the Reynolds number based on the diameter of the cavity, R_d. Velocity profile measurements showed that for the cases of $d/h > 1$ an increase in skin friction drag was experienced with respect to a smooth surface, but for $d/h \leq 1$ the drag increment was almost negligible and in some cases it was lower than that of a smooth surface by up to 10%. Measurements along the spanwise plane showed the presence of organised transverse velocity components which bear some resemblance with the flow over riblets. The skin friction drag appears to be a strong function of R_d, where for $R_d > 5500$ a drag increment is experienced which could potentially be due to shear layer breakdown and more production of turbulence.

1. INTRODUCTION

From the pioneering studies of Nikuradse [15] surface roughness or other excrescences such as grooves and cavities are major sources of skin friction drag in turbulent boundary layers in wall bounded flows. Nikuradse also derived a set of semi-empirical relations to assist in estimating the drag increment with respect to a hydrodynamically smooth surface. Since then a vast amount of research has been conducted which supports the findings of Nikuradse and also provides further insight into the physical mechanisms, improving the initial semi-empirical and later numerical models. A comprehensive review of turbulent flow over roughness was presented by Jiménez [11]. A new perspective was introduced by Walsh [19] in the 1980s who demonstrated that grooves, or 'riblets' aligned with the streamwise direction, if sufficiently submerged in the viscous sub-layer, could reduce the viscous drag by almost 10%. Additional experimental validation was provided by Choi [5] in the late 1980s including details of the physical mechanism behind riblet control and further studies followed, by Berchert and co-workers [2], [3] and [4], over a period a more than two decades using highly viscous fluid to assist in resolving the flow structures.

In a reversal of bio-inspired thinking it was thought that, if the riblet mechanism was effective then nature would have got there first and this triggered the idea that the mechanism might already be present on the skin of fast swimming sharks. Recent studies by Dean and Bhushan [7] focused on measurements on surfaces emulating the texture of shark skin together with the addition of mucus within the grooves. They postulated that the mucus presents an added benefit. Further insight into the physical drag reduction mechanism was provided analytically by Luchini et al. [14]. The review of Karniadakis and Choi [13] described riblets as fences aligned with the streamwise direction which hinder the spanwise propagation of the coherent longitudinal structures during the sweep event, where the high momentum fluid moves towards the wall as a result of turbulent mixing, leading to a reduction in the wall shear stress.

Most of these studies have dwelled mainly on riblets, however Tani [17] suggested that randomly distributed roughness could also lead to similar drag reduction benefit without explaining the mechanism in detail. Later, Sirovich and Karlsson [16] demonstrated that a staggered array of discrete protrusions with a lambda-shaped cross-section could also reduce skin fiction drag, whereas aligned protrusions led to a drag increment. They postulated that the physical mechanism responsible for drag reduction was completely different to that of riblets but could be similar to the mechanism that exists during spanwise wall oscillation which modifies the phase of obliquely propagating structures, altering the net down-

wash of high momentum fluid. A more recent study by [18] showed that rounded edges dimples can also help in reducing skin friction drag. In their case, even if the Reynolds number based on the diameter was relatively high, the flow within the dimples was still attached and the drag reduction mechanism was through the generation of a converging-diverging flow.

The current investigation was initially focussed on understanding the drag penalty of staggered discrete circular cavities, as typically found in acoustic liners in turbofan engines, but following unexpected drag trends, developed into a study of the flow structure induced by the cavities which may be analogous to surface protrusion effects reported by Sirovich and Karlsson. The skin friction drag benefit claimed here could potentially be attractive to the aerospace and general transport industry, and for pipe flow and channel flow applications.

2. THE EXPERIMENT

The experiment was conducted in the T2 low speed wind tunnel at the Handley Page laboratory at City, University of London which has a working section of $0.8m \times 1.12m \times 1.8m$. The experimental boundary layer was generated on a wooden flat plate model with an elliptical leading edge, of ratio 5:1. The model was also equipped with a trailing edge flap to control the pressure gradient over the plate. The initial laminar boundary layer was tripped using a $0.2mm$ trip-wire placed at $100mm$ downstream of the leading edge and its effectiveness in generating a turbulent boundary layer was confirmed by the hot wire signal. A streamwise row of surface pressure tappings, offset by $100mm$ from the model centreline, was used to check the pressure gradient. Embedded in the plate was a square cavity of side $192mm$ and depth $18mm$. The cavity was recessed to accommodate a set of a perforated acrylic panels such that the surface of the panels was flush with the surface of the flat plate. The thickness of the panels, h, and perforation spacing, s, were constant at $3mm$ and $20mm$ respectively and the diameter of the perforations, d, varied from $2mm$ to $5mm$. The rig is shown in Fig. 1, which also shows the surface mounted, single axis traverse system used to capture the velocity profiles of the boundary layer using hot wire anemometry.

King‘s law was applied for the hot wire calibration and the velocity profile was captured using the surface mounted traverse which has a resolution of $5\mu m$ per step, together with the digital-optical system, developed by Gowree et al [10], to position the hot wire very close to the surface of the plate. The combination of this traverse probe and the optical alignment system has been shown to deliver very accurate values for boundary layer integral quantities. As the traverse system had to be permanently fixed to the surface of the model, the hot wire traverse was limited to a single location along the centreline of the model and downstream of the final row of the cavities, at x=730mm from the leading edge. This corresponds to 20mm downstream of the last row of cavities. From figure 2, the centreline passes over the centre of the middle row of cavities and therefore care was taken so that the measurement station was not in the near wake of the cavity. From the flow visualisation in figure 9, at a freestream speed of 15m/s the near-field, large structures seemed to be dissipated at approximately 3 diameters downstream of the cavity and therefore a recovery region of 20mm downstream of the whole was chosen.

To explore the structure of the flow along the spanwise plane, three-component LDA measurements were performed using a tri-axis traverse system which assisted in the measurement of a larger spatial domain than could be captured by the hot wire. A DANTEC Dynamics LDA system was used while operating in backward scatter mode. Based on the focal length of the lenses, a probe volume of approximately $120 \times 120 \times 2600\mu m$ was obtained. All the measurements were made in the transverse and wall-normal planes, y and z respectively, at $x = 730mm$. This was approximately $20mm$ downstream of the last row of cavities as shown schematically in Fig. 2. The centreline of the plate corresponds to $y = 0mm$ which was also the centreline of the middle row of holes. Surface oil flow visualisation was also performed to obtain a qualitative understanding of the flow physics in the vicinity and downstream of the cavities. The experiment was conducted with the perforations first sealed on the reverse side of the acrylic sheets, as shown on the bottom right of Fig. 1, and secondly open to a single plenum underneath the perforated panel.

The desired zero pressure gradient condition within the experimental domain was first confirmed using an unperforated plate over the cavity. Fig. 3 shows the development of the freestream velocity in the streamwise direction. This result confirmed that the $x = 730mm$ measurement station was in the zero pressure gradient region.

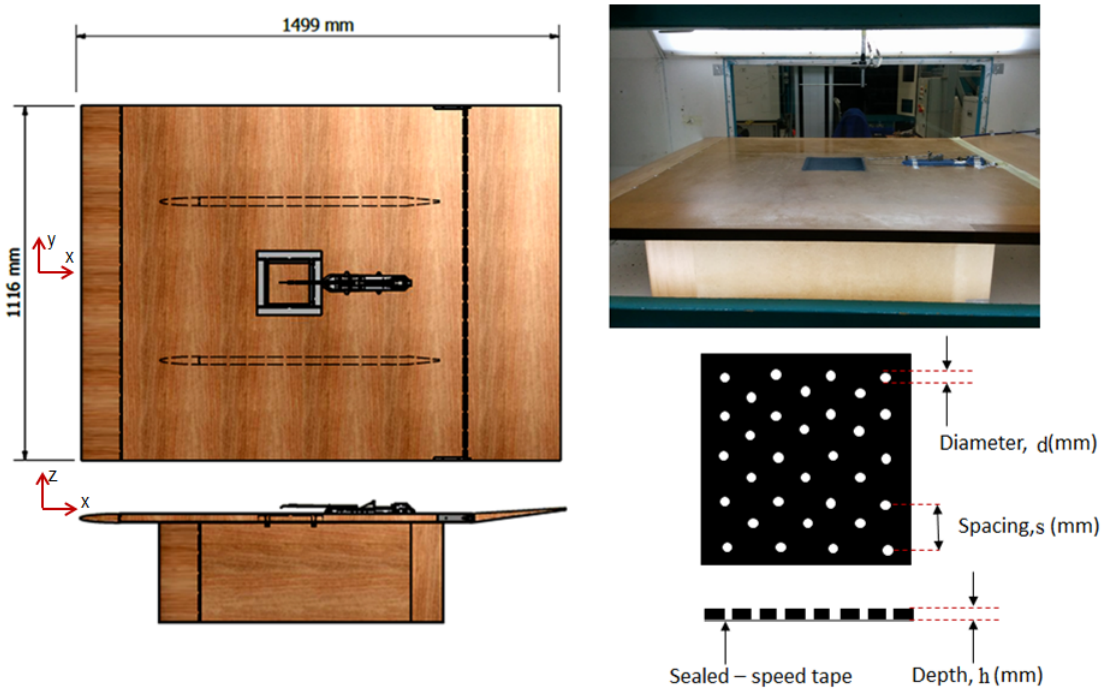

Figure 1: The top and side view of the flat plate (left) and the plate mounted in test section of the wind tunnel (top right). The bottom right figure is a schematic representation of perforated panel to show the distribution of the cavities.

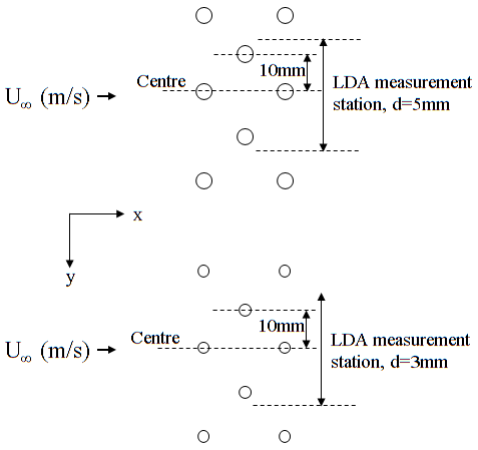

Figure 2: Schematic representation of the top-view of the LDA measurement station

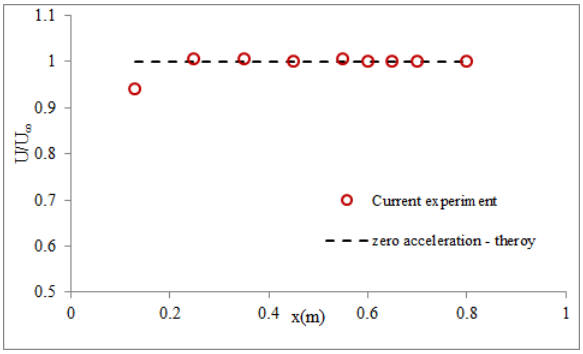

Figure 3: The streamwise velocity gradient along the flat plate

3. RESULTS

3.1 Unperforated plate

The initial hot wire traverse was made on the baseline, unperforated panel for later comparison with the results from the perforated cases. From the velocity profiles captured on the smooth surface the skin friction was determined using Clauser's chart technique [3], for which the log-law was defined using a von Karman constant of 0.41.

The resulting shear stress was used to express the velocity profiles in wall units as shown in Fig. 4 where the profiles can be seen to be consistent with the above choice of von Karman constant and the standard y-intercept of 5.1. From the velocity profiles the boundary layer integral quantities were calculated, including the skin friction coefficient which is plotted against Reynolds number, based on the momentum thickness, θ, in Fig. 5. Note that due to the proximity of the hot wire with the surface the first few measurements were prone to heat transfer effects and were discarded during the calculation of the momentum thickness. Although the most obvious points were not inlcuded in the profile, in figure 4 this effect is still seen in the first measure-

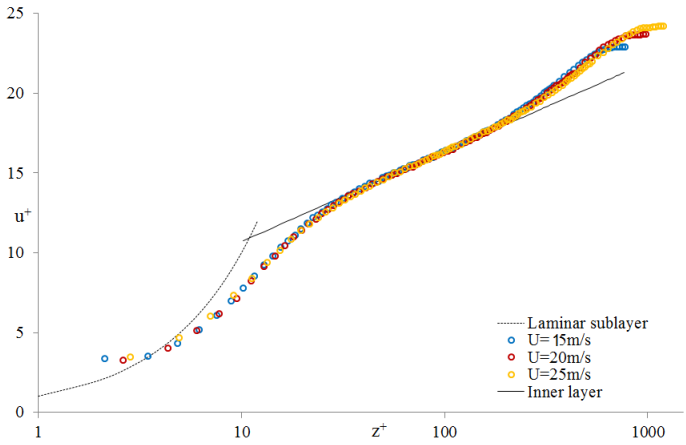

Figure 4: Velocity profiles along unperforated plate at $x = 730mm$. The universal log law is defined by $z^+ = (1/0.41)\,ln\ u^+ + 5.1$

ment points. The results from the smooth case are compared with the semi-empirical relation given by Gaudet [8] and the DNS results from Jimenez et al. [12]. At lower R_θ the current experimental results show closer agreement with the DNS results; however, throughout the whole range of R_θ tested, the agreement was within 2% of Gaudet's results.

3.2 Perforated plate

The local skin friction on the perforated panel walls was determined using Clauser's [6] chart technique for the same value of von Karman constant. These results are also presented in Fig. 5. The obtained skin friction coefficients were then used to express the velocity profiles in wall units as shown in Fig. 6. For cavities with $d > 3mm$, the downward shift in the logarithmic profile, shows an increase in the local skin friction similar to the behaviour noticed in turbulent boundary layers over rough walls. This behaviour is in line with the observations of Nikuradse [15] and Clauser [6] and many others, summarised by Jimenez [11]. However, the upward shift in the profile for the $d \leq 3mm$ case suggests that a reduction in local skin friction is encountered. This this trend is also clear in Fig. 5, which also shows that the effect of removing the seal under the perforations is small.

From dimensional analysis, the ratio d/h and the Reynolds number based on the diameter of the cavity, R_d, are considered to be the influential geometrical parameters and the skin friction obtained from Clauser's technique is plotted against these dimensionless groups in Fig. 7. From the left hand side of Fig. 7 a well-defined trend is present, suggesting that for $d/h \leq 1$, a drag reduction of up to 10% could be obtained, while for $d/h > 1$ there is a correspondingly sharp drag rise. However, the right hand side of Fig. 7 suggest that the dependence on Reynolds number is weak. The accuracy and reliability of Clauser's technique in the presence of the cavities are questionable due to the modification of the characteristic of the wall in the presence of coherent structures generated by the cavities. Therefore other physical quantities of the boundary layer which is correlated to the skin friction drag were further investigated.

For a zero pressure gradient flow, the momentum integral equation can be reduced to

$$\frac{d\theta}{dx} = \frac{c_f}{2} \tag{1}$$

It can be extended to a case of spanswise periodic mean flow based on Ashill and Smith's [1] formulation of the 3D momentum integral equations and the assumption presented in the Appendix.

So the effect of the cavities on the turbulent skin friction can also be quantified by considering the momentum thickness, θ, as presented in Fig. 8. The change in momentum thickness is a measure of the average change in skin friction over the length of the plate, in contrast to the velocity profiles which indicate local skin friction values. $\Delta\theta/\theta$ is seen to increase with increasing d/h and but the rate of change is less steep than $\Delta c_f/c_f$ (Fig. 7). Moreover, for the lowest speed tested, $U = 15m/s$, a reduction in θ can be observed for all the ratios of d/h tested. This observation contradicts the trend from Fig. 6 and 7, where a skin friction penalty was observed for the cases of $d > 3mm$. The relation between $\Delta\theta/\theta$ and R_d is more consistent and there seems to exist a particular regime at $R_d < 6000$ where the skin friction reduction is observed. In Fig. 8 an anomalous data point for the case of U=20m/s, with sealed holes has

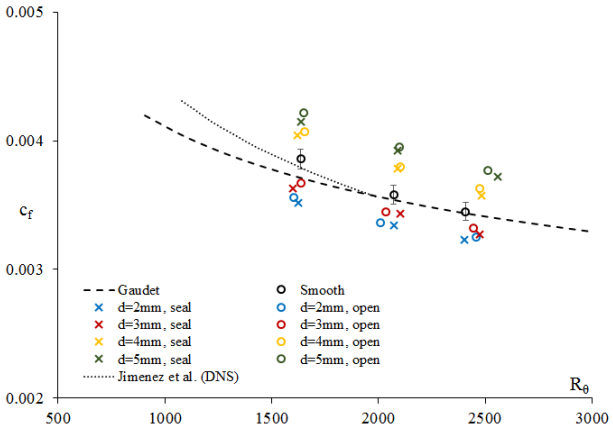

Figure 5: The local skin friction on the different of surfaces tested, where the baseline smooth case is compared with the DNS study of Jimenez [7] and the semi-empirical relation given by Gaudet [8]

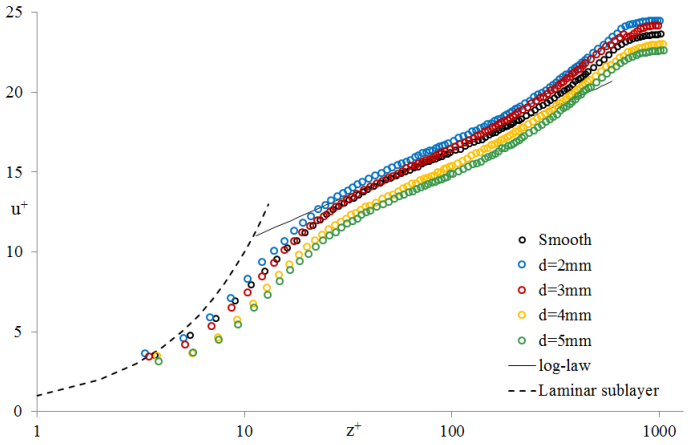

Figure 6: Velocity profiles above perforated plate at $x = 730mm$,for a freestream velocity of $15m/s$ and the cavities sealed at the bottom. The universal log law is defined by $z^+ = (1/0.41)\,ln\;\; u^+ + 5.1$

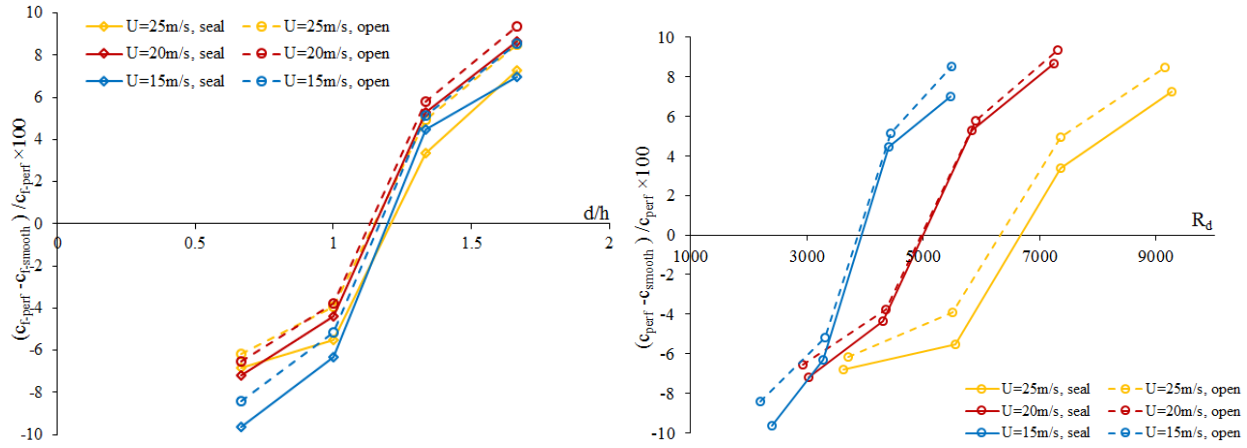

Figure 7: The percentage difference in the local skin friction drag, c_f, between the perforated and smooth cases as a function of the ratio, d/h $(left)$ and R_d $(right)$.

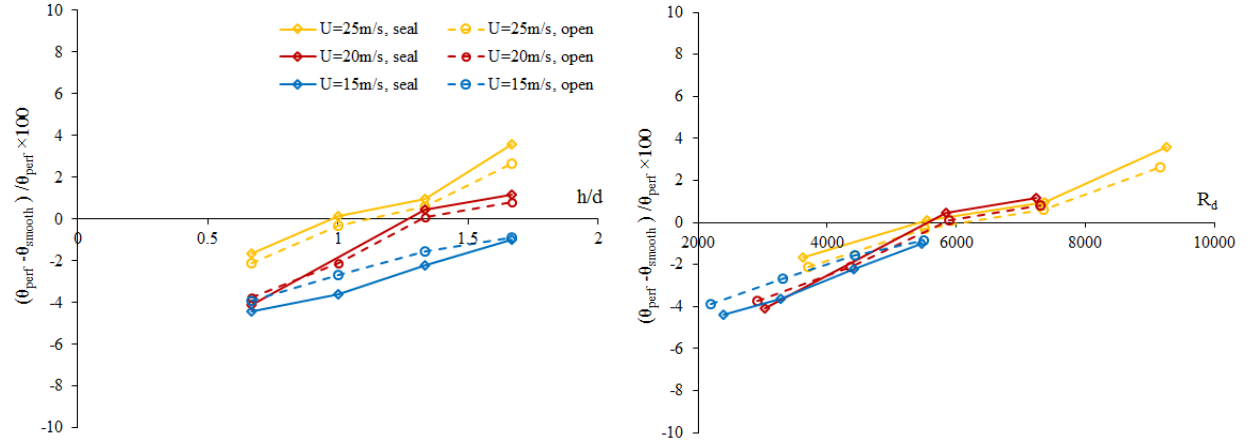

Figure 8: The percentage difference in momentum thickness, θ, between the perforated and smooth cases as a function of the ratio, d/h (left) and R_d (right).

been omitted.

So far the skin friction drag has been treated purely from a mean flow basis. Further evidence could be obtained by analysing the RMS of the fluctuating components and from the hot-wire measurements the streamwise component, u', was captured and is presented in figure 9. At a freestream velocity of $15m/s$, the peaks in u' for $2mm$ and $5mm$ cavities are slightly lower than that of the smooth case, this therefore confirms that skin friction is lower for these cases. As opposed to the case of $25m/s$ where the peak of the $5mm$ cavities was higher than the $2mm$ and the smooth cases, which were in turn very similar. It is also interesting to note that at $15m/s$, in the outer region of the boundary layer, $y/\delta > 0.6$, the intensity of u' in the presence of the cavities is lower than the smooth case, whereas at $25m/s$ they are all quite similar. In the inner layer region, $y \approx 0.2$, for the cavities, $d = 2mm$, and smooth case u' are very similar whereas that for $d = 5mm$ is higher. With increasing freestream speed the intensity in u', should increase further and will merge with the peak into a plateau similar to the case of very large roughness.

3.3 Topology of surface streamlines

The surface oil flow patterns in the vicinity and downstream of the cavities are shown below in Fig. 10. The streamline patterns are consistent with the formation of vortical structures around the cavities. For the three cases on the upper left of Fig. 10 a drag reduction was observed whereas for the three cases to the lower right a drag penalty was observed. The development of the streamline patterns as hole size and freestream velocity are increased is rather subtle, but for the case where the greatest drag reduction was observed (d=3mm, at 15m/s) there are clear signs of lateral velocities component in the surface streamline.

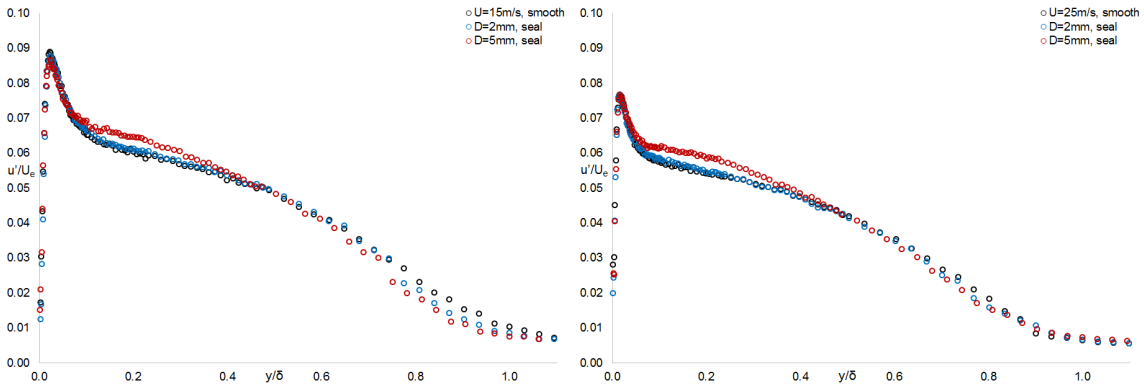

Figure 9: The normalised rms of the fluctuating streamwise component, u'/U_e, captured by the hot wire at a frestream velocity of 15m/s (left) and 25m/s (right), for the smooth case and the perforated cases of $d = 2mm$ and $d = 5mm$.

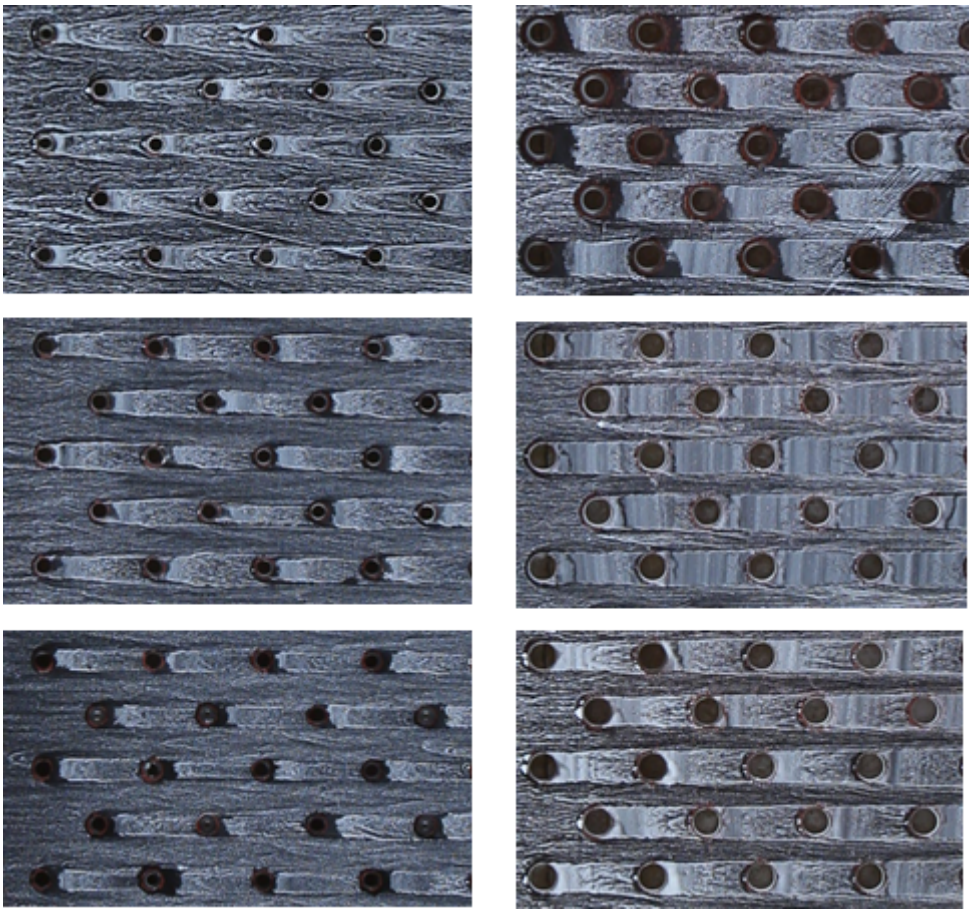

Figure 10: Surface streamline visualisation of the flow around the circular cavity of d=3mm (left) and d=5mm (right). Where the freestream velocity from top to bottom are from 15, 20, 25m/s respectively

3.4 3D LDA measurements

The LDA data was filtered so as to discard all measurements with a validation level less 30%. A spline fit algorithm was employed to interpolate the velocity contours, resulting in a more organised representation of the turbulence structures. The normalised streamwise velocity components are shown in Fig. 11 for the cases of $d = 3mm$ on the left and $d = 5mm$ on the right, for $R_d \approx 5000$ and $R_d \approx 8500$ respectively at $U_\infty \approx 22.5m/s$. Note that at this Reynolds number, a drag reduction was observed for $d = 3mm$ whereas a drag penalty was observed for $d = 5mm$ in comparison to a smooth surface. The streamwise velocity components shown in Fig. 11 reveal a region of lower momentum flow near the wall at

$y = \pm 5mm$. As shown in Fig. 2 the hole centres lie at $y = 0mm$ and $y \pm 10mm$. The pockets of low streamwise momentum fluid are therefore consistent with a secondary flow induced by the adjacent legs of the neighbouring hole vortices. The sense of rotation is to lift low momentum fluid in between the holes and to bring down high momentum fluid behind the holes which is consistent with the oil flow patterns seen at the top left of Fig. 10. The rms of the fluctuating streamwise and transverse velocity components are shown at the top and bottom of Fig. 12 respectively, for $d = 3mm$ (left) and $d = 5mm$ (right). The secondary flow from the hole vortices appears to lift the turbulent near wall flow away from the surface for the case of $d = 3mm$ but not for $d = 5mm$. This is consistent with the observed drag reduction for $d = 3mm$.

4. DISCUSSION

The skin friction measured for the baseline smooth surface agrees well with the universal log-law, the skin friction results obtained from DNS and semi-empirical results, all shown in Fig. 4. This provides confidence in the measurement technique and the data analysis process. The uncertianty in the skin friction drag inferred from the Clauser's technique and the momentum deficit, $d\theta$ rely on the accuracy of the velocity profiles measurements. Gowree et al. [10] showed that the traverse mechanism could comfortably provide a single step displacement of $5\mu m$ at an accuracy lower than $\pm 5\%$. Further error analysis by Gowree [9] demonstrated that the optical alignment allowed the positioning of the hot-wire with an accuracy of $\pm 2.5\mu m$ with respect to the wall and within a confidence level of 95%, the whole boundary layer traverse can be captured at a total relative uncertainty of 3.9%. This was for turbulent velocity profiles with a maximum thickness of 3mm, so here it will be fair to assume that the confidence level in the velocity profile measurement is even higher and therefore a lower total relative uncertainty can be expected as the boundary layers are about 4 to 5 times thicker. From Fig. 6 the upward shift of the inner layer for the cases where $d < 3mm$ suggests that the local skin friction is reduced. This is supported by the fluctuating velocity components presented in Fig. 12. We do not believe that this observed skin friction reduction over some types of perforated surfaces has been reported previously. Small differences in skin friction between the opened and sealed cavities are thought to be due to low levels of pressure fluctuation, resulting in forced momentum transfer into the plenum under the perforated sheet. Larger magnitudes of unsteady transpiration (e.g in the presence of strong acoustic forcing) would be expected to lead to large skin friction increments which were clearly not observed in the present work. Using the Clauser chart technique, a skin friction reduction was observed for a cavity diameter to height ratio, $d/h < 1$, but a different trend was obtained from the momentum thickness results which suggested drag reduction for all $R_d < 6000$. We note here that the Clauser chart technique might be restricted to cases where the log-law constants do not differ from the equivalent smooth wall values. From the hot wire measurments the peaks in the intensity of the fluctuating streamwise component, u', for the cavities in this regime were lower than the relative smooth cases and this also supports the drag reduction observed here.

Surface flow visualisations (Fig. 10) revealed the spanwise non-uniformity of the flow and the presence of transverse velocity components and streamline patterns consistent with vortical structures generated by the cavities. The effect of the spanwise variation on the local skin friction was checked by plotting the velocity profiles from the LDA measurements on a Clauser chart as shown in Fig. 13. The LDA velocity profiles suggest that the spanwise variation in skin friction was small and symmetrical suggesting that drag reductions extended over the whole span of the perforated plate and is not just a localised benefit observable in the wake of the trailing vortex. We note that for the case of $d = 5mm$ shown on the right of Fig. 13, no significant variation can be seen between the profiles at the three spanwise positions.

The LDA measurements were useful in explaining the footprint of the surface streamline shown in 10 and in capturing the effect on the boundary layer turbulence, offering insight into the possible mechanism of drag reduction. Referring back to the Introduction, in previous studies skin friction reduction had been achieved by manipulating the transverse velocity component either by using riblets, spanwise oscillation or randomly distributed protrusions. According to Berchert et al. [6], a reduction in the fluctuating transverse or spanwise component near the wall will result in a reduction in turbulent energy production and hence lower shear stress. With the current limited results one can only speculate that the reduced transverse velocity fluctuations at $y \pm 5mm$ for the $d = 3mm$ case could be a contributing factor to the observed skin friction reduction. These features were not visible in the $d = 5mm$ case.

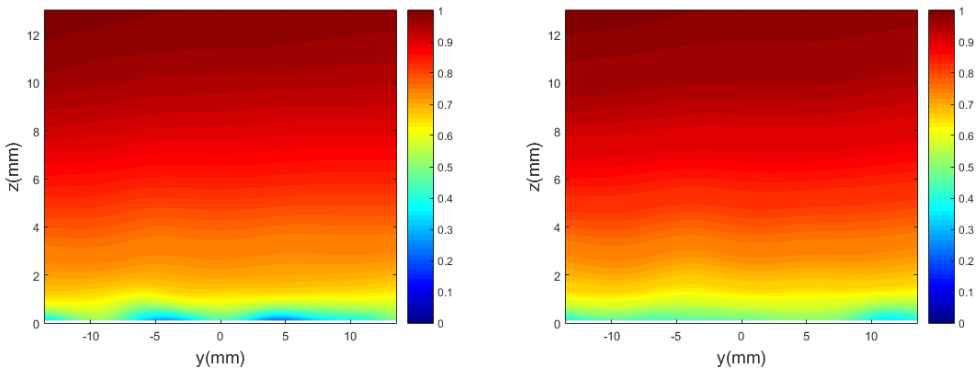

Figure 11: The normalised mean streamwise velocity component, u/U_e for the $d = 3mm$ (left) and $d = 5mm$ (right), with $R_d \approx 5000$ and $R_d \approx 8500$ respectively.

For $d = 3mm$ both the mean streamwise and fluctuating transverse velocity components are organised in a similar fashion to that of the flow over riblets, suggesting that the drag reduction mechanism could be similar. However, the scenario present in the case studied by Sirovich and Karlsson cannot be ruled out. For the $d = 5mm$ case Fig. 12 shows the transverse velocity fluctuations to be higher in magnitude and further away from the wall than the streamwise velocity fluctuations which is perhaps associated with unsteadiness in the vortical structures which may explain the Reynolds number dependence of the secondary flow.

5. CONCLUSION

Measurements of the low speed flow field around staggered array of three dimensional cavities have demonstrated a potential passive method for skin friction drag reduction. Following a parametric study, the drag benefit was observed to be limited to some extent by the ratio d/h and to be a strong function of the Reynolds number based on the diameter of the cavity, R_d. Surface flow visualisation and LDA measurements across a spanwise plane indicated the presence of vortices shed by the cavities which, for the cases exhibiting reduced skin friction, organise the transverse fluctuating velocity in a similar fashion to riblets. A benefit of staggered cavities would be a lower excrescence drag penalty in comparison to that from riblets.

Further work should explore in greater detail the development of the flow structures with Reynolds number and/or cavity spacing and geometry to understand the limitation on the mechanism.

ACKNOWLEDGEMENTS

The authors would like thank the Innovate UK for their financial support to the SANTANA project under grant No. 113001.

APPENDIX

The analysis applicable here is for the boundary layer flow under a straight streamline in a zero-pressure-gradient, incompressible, three-dimensional flow: a rare occurrence, but one example would be the viscous layer between a two-dimensional inviscid flow and a three-dimensional surface, such as the perforated plate of the current study. The three-dimensional momentum integral equations can be obtained from a number of sources, but here we follow Smith and Ashill (RAE TR 83053) and cite only the momentum integral equation in the streamwise direction, modified to allow for zero pressure gradient, incompressible flow and zero streamline curvature:

$$\frac{\partial \theta_{11}}{\partial s} + \frac{\partial \theta_{12}}{\partial n} = \frac{\tau_{w1}}{\rho U_e^2} \tag{2}$$

Here s and n are respectively the directions parallel to, and normal to, the external streamline; U_e is the inviscid velocity at the boundary layer edge; ρ is the density of the incompressible fluid; and τ_{w1} is the wall shear stress in the direction of the external streamline. The integral scales are defined by:

$$\theta_{11} = \int_w^e \frac{u}{U_e}\left(1 - \frac{u}{U_e}\right) dz \tag{3}$$

$$\theta_{11} = \int_w^e \frac{v}{U_e}\left(1 - \frac{u}{U_e}\right) dz \tag{4}$$

where u and v are respectively the velocity component in the s and n directions and w and e respectively indicate conditions at the wall and at the

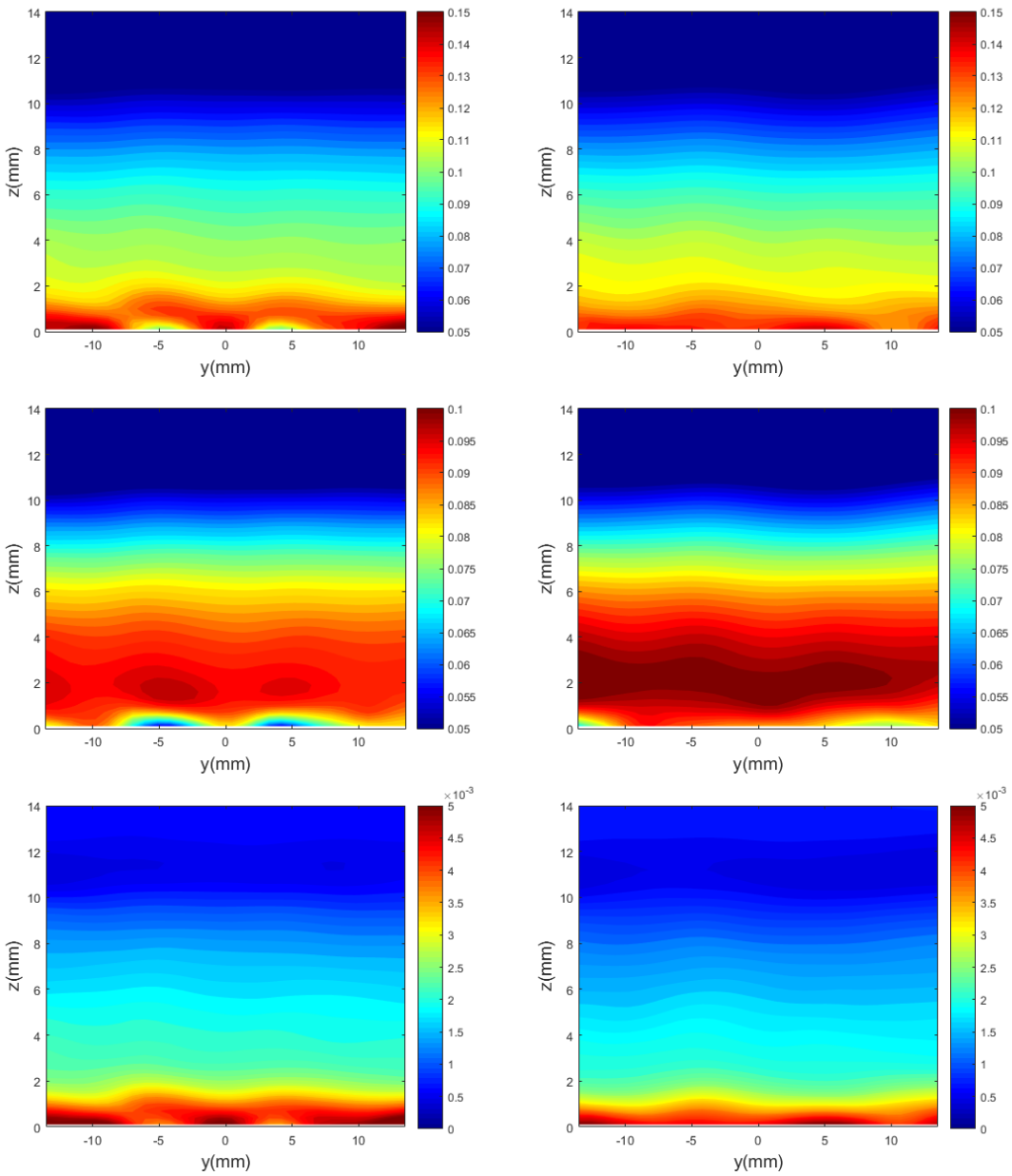

Figure 12: The normalised rms streamwise velocity, u'/Ue (top), transverse v'/Ue (centre) velocity components and bottom $(u'^2 - v'^2)/U_e^2$, for the $d = 3mm$ (left) and $d = 5mm$ (right), with $R_d \approx 5000$ and $R_d \approx 8500$ respectively.

boundary layer edge. Additional terms are included by Ashill and Smith arising from streamwise pressure gradient, from streamline curvature in the inviscid flow and from gradients of density, all of which are absent in the present situation.

In the control volume analysis which can be used to derive both the differential and integral boundary layer equations, the term

$$\frac{\partial}{\partial n}\left[\int_w^e \frac{v}{U_e}\left(1-\frac{u}{U_e}\right)dz\right] \qquad (5)$$

represents the net change in streamwise momentum due to the gradient in lateral convection of streamwise momentum across the sides of the control volume. Any net outflow of streamwise momentum due to the normal (crossflow) velocity component, v, would result in an inflow of momentum to the neighbouring control volume and vice versa. Thus, for a flow which is two-dimensional from the macroscopic perspective, any imbalance in lateral flow of momentum would diminish in importance as the control volume was extended across the flowfield. In the present context, the significance of this effect can be determined by the variation of momentum thickness, θ_{11}, in the lateral direction (i.e. across the stream). Assuming that this variation is very small, we can

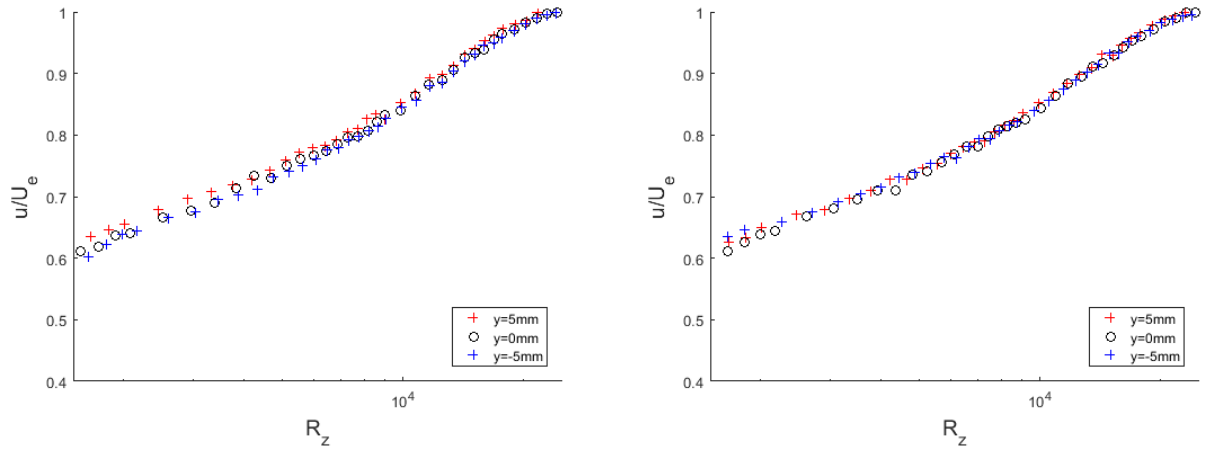

Figure 13: Velocity profiles expressed as Clauser chart, for three position along the spanwise plane located at x=730mm, for the case of d=3mm (left) and d=5mm (right) with $R_d \approx 5000$ and $R_d \approx 8500$ respectively. R_z, represents the Reynolds number based on the local height, z, with respect to the wall.

then apply the two-dimensional form of the momentum integral equation

$$\frac{\partial \theta_{11}}{\partial s} = \frac{\tau_{w1}}{\rho U_e^2} \tag{6}$$

effectively treating the localised effects of the three-dimensional surface features as a modifier to the mean, two-dimensional wall shear stress, θ_{11}.

REFERENCES

[1] P. R Ashill and P. D Smith. An integral method for calculating the effects on turbulent boundary-layer development of sweep and taper. *The Aeronautical Journal (1968)*, 89(882):4354, 1985.

[2] D. W. Bechert and M. Bartenwerfer. The viscous flow on surfaces with longitudinal ribs. *Journal of Fluid Mechanics*, 206:105–129, 009 1989.

[3] D. W. Bechert, M. Bruse, and W. Hage. Experiments with three-dimensional riblets as an idealized model of shark skin. *Experiments in Fluids*, 28(5):403–412, 2000.

[4] D. W. Bechert, M. Bruse, W. Hage, J. G. T. van der Hoeven, and G. Hoppe. Experiments on drag-reducing surfaces and their optimization with an adjustable geometry. *Journal of Fluid Mechanics*, 338:59–87, 005 1997.

[5] Kwing-So Choi. Near-wall structure of a turbulent boundary layer with riblets. *Journal of Fluid Mechanics*, 208:417–458, 11 1989.

[6] Francis H Clauser. Turbulent boundary layers in adverse pressure gradients. *Journal of Aeronautical Sciences*, 21(2):91–108, 1954.

[7] Brian Dean and Bharat Bhushan. Shark-skin surfaces for fluid-drag reduction in turbulent flow: a review. *Philosophical Transactions of the Royal Society of London A: Mathematical, Physical and Engineering Sciences*, 368(1929):4775–4806, 2010.

[8] L. Gaudet. Experimental investigation of the turbulent boundary layer at high reynolds numbers and a mach number of 0.8. *The Aeronautical Journal*, 90(893):83–94, 003 1986.

[9] E. R Gowree. Influence of attachment flow on form drag, 2104.

[10] E R Gowree, C J Atkin, and S Gruppetta. A simple digital-optical system to improve accuracy of hot-wire measurements. *Measurement Science and Technology*, 26(9):095303, 2015.

[11] J Jiménez. Turbulent flows over rough walls. *Annual Review of Fluid Mechanics*, 36(1):173–196, 2004.

[12] Javier Jiménez, Sergio Hoyas, Mark Phil Simens, and Yoshinori Mizuno. Turbulent boundary layers and channels at moderate reynolds numbers. *Journal of Fluid Mechanics*, 657:335–360, August 2010.

[13] G. E. Karniadakis and Kwing-So Choi. Mechanisms on transverse motion in turbulent wall flows. *Annual Review of Fluid Mechanics*, 35(1):45–62, 2003.

[14] Paolo Luchini, Fernando Manzo, and Amilcare Pozzi. Resistance of a grooved surface to parallel flow and cross-flow. *Journal of Fluid Mechanics*, 228:87–109, 007 1991.

[15] J Nikuradse. Laws of flow in rough pipes. Technical report, NACA TM 1292, 1933.

[16] L Sirovich and S Karlsson. Turbulent drag reduction by passive means. *Nature*, 388:753–755, 1997.

[17] Itiro Tani. Drag reduction by riblet viewed as roughness problem. *Proceedings of the Japan Academy, Series B*, 64(2):21–24, 1988.

[18] M. van Nesselrooij, L. L. M. Veldhuis, B. W. van Oudheusden, and F. F. J. Schrijer. Drag reduction by means of dimpled surfaces in turbulent boundary layers. *Experiments in Fluids*, 57(9):142, Aug 2016.

[19] M. J. Walsh. Drag characteristics of v-groove and transverse curvature riblets. *Progress in Astronautics and Aeronautics*, 72:168–184, August 1980.